The Juventas GNC Subsystem, Autonomous Landing on the Surface of the Binary Asteroid Dimorphos

Ovejero Provencio D.[(1)], Moreno Villa V.M.[(1)], Stancu F.[(2)], Plamadeala A.[(2)], Nistal Reñones M.[(1)], Domínguez Castillo A.[(1)], Plevier C.[(3)], Scoubeau M.[(3)], da Silva Pais Cabral F.[(4)]

[(1)] GMV Spain, Tres Cantos, Spain, daniel.ovejero@gmv.com, vimoreno@gmv.com, marcos.nistal.renones@gmv.com, adalberto.dominguez.c@gmv.com
[(2)] GMV Romania, Bucharest, Romania, fstancu@gmv.com, andrei.plamadeala@gmv.com,
[(3)] Gomspace Luxembourg, Esch-sur-Alzette, Luxembourg, capl@gomspace.com, mesc@gomspace.com
[(4)] GMV, Lisboa, Portugal, francisco.cabral@gmv.com

ABSTRACT

Juventas is a deep space 6U XL CubeSat with the objective of performing a scientific and technological demonstration mission, aiming for the characterization of the binary asteroid Didymos, and its small companion Dimorphos. Juventas takes part in the Hera mission as one of the two CubeSats that will be released in the asteroid's proximities. As experimental payload, Juventas is designed to take higher risks than his mothercraft and get closer to the asteroids, and eventually perform an autonomous landing on Dimorphos.

Juventas will be inserted into a special set of orbits, called Self-Stabilized Terminator Orbits (SSTO). The existence of this special type of in which the solar radiation pressure (SRP) perturbation cancels the gravitational pull of the central body. The high latency of the information along with the small distances to the target causes great uncertainties in the predicted CubeSat state. Hence, to prevent the asteroid from abandoning the camera's field of view, fast onboard attitude corrections must be commanded by the GNC system to achieve continuous imaging of the asteroid.

Juventas' GNC is designed to be able to land on the surface of Dimorphos once the radar observations from the SSTOs have been performed. The landing comprises a controlled touchdown using the autonomous GNC system and a series of uncontrolled bounces until Juventas rests on the asteroid's surface. The highly perturbed dynamics together with the small size of the target make the landing the most challenging operation that Juventas will face.

The landing of Juventas on Dimorphos presents a series of difficulties that can only be tackled by the autonomous GNC implementation. Firstly, the insertion manoeuvre from the SSTO has a high uncertainty due to the long turnaround times. This insertion is corrected by the GNC which allows a flexible solution for the definition of the manoeuvres, being flexible to the number of manoeuvres and their execution times. Each of the manoeuvres employs the estimated instantaneous state estimation of the filter, using data fusion techniques that combine Image Processing of NAVCAM images for line-of-sight estimation and ranging with a laser altimeter. Consequently, braking manoeuvres are performed when the estimated SC approaches the surface of Dimorphos.

The GNC is also flexible to the moment of execution of the insertion phase, being able to compute the optimal position with respect to the orbital plane to perform the manoeuvres. Secondly, Juventas should land at a reduced velocity to guarantee that the CubeSat will not bounce back and escape the gravity field of Dimorphos.

This paper will include the consolidated strategies of the GNC designed for the Juventas landing strategy. The focus will be directed towards the modes and functions necessary to operate the CubeSat autonomously.

1 INTRODUCTION

Juventas CubeSat is one of the two CubeSats that are part of the Hera mission. The Hera spacecraft will be launched in October 2024 and rendezvous in late 2026 December with the binary asteroid (65803) Didymos and in particular its moon, Dimorphos, which was impacted by NASA's DART spacecraft on 2022 September 26 as the first asteroid deflection test. Juventas will be *piggybacked* until the mother spacecraft finishes its ECP (Early Characterisation Phase), when it will be released at around 30 km distance to Didymos. Juventas will be inserted into a circular orbit around Didymos where it will carry out the bulk of its operations. It will be during this time, in which the JURA instrument will take measurements of Dimorphos. The selected orbits for this task are two self-stabilized terminator orbits (SSTO), with the first one at 3.3 km from Didymos and the second at 2 km. The SSTOs, also called photo-gravitational orbits, have been studied for a large number of missions as in [1] and [2]. The interest of these orbits lies in the scientific return obtained from them and the reduced number of operations required. Juventas operations will last around 3 months, with near 1 month dedicated to each SSTO orbit.

For the end of life of the spacecraft, a landing on Dimorphos has been selected. Landing on Dimorphos would be a major achievement for the European space industry and ESA as it would be the first soft landing performed by a European space probe on an asteroid and more specifically, on a binary asteroid system and the smallest asteroid ever visited. Few landings on asteroids have been performed by space probes, the first one being performed by NEAR Shoemaker [3] (NASA) which visited the asteroid (433) Eros and successfully landed on February 12, 2001. This probe, similar to Juventas, was not designed as a lander and was eventually deactivated once it had performed the touchdown. One key difference though is that NEAR did not feature any payload dedicated the landing phase, whereas Juventas includes a small gravimeter (GRASS [4]) to measure Dimorphos gravity field which will be turned on during the last phases of the descent. A different approach was taken for successive asteroid landing missions, for which not a real "landing" was proposed, but a soft touch followed by a sample collect and return back to Earth. This is the case for the JAXA's Hayabusa [5], which touched (25143) Itokawa in 2005, and Hayabuse 2 [6], which touched (162173) Ryugu in 2019, and finally OSIRIS-Rex [7] (NASA) that, in 2020, landed on (101955) Bennu which was the smallest object to be orbited by a spacecraft.

Juventas GNC has been developed and validated by GMV.

2 JUVENTAS GNC ARCHITECTURE

Juventas uses optical (images taken from a wide-angle camera provided by VTT) and range measurements (from Jenoptik's laser rangefinder DLEM family) in a co-boresight configuration to navigate around Didymos and Dimorphos. The images are fed to an image processing algorithm which estimates the centre of the asteroid in pixels. These measurements are then used in an extended Kalman filter (EKF) that outputs the spacecraft state (position and velocity) as well the different time-varying biases in accelerations and sensor measurements that are included in the augmented state. During nominal operations, Juventas will be pointing to nadir with the solar panel direction perpendicular to the Sun. This pointing is computed by the attitude guidance and has a high degree of autonomy, not requiring any attitude profile from ground, as it uses the position estimation from the filter and on-board ephemeris. For the translational guidance, Juventas uses pre-computed from

ground during nominal operations with the flexibility of providing a reference trajectory via state transition matrices (STM) to update values on-board.
Regarding the landing, this requirement has been a design driver as this mission phase introduces several constraints that shape the different algorithms to be used, mainly regarding the image processing and the translational guidance. These constraints are explained through the following points:

- The difference in asteroid geometry between Didymos and Dimorphos. Didymos is more sphere-like while Dimorphos has a clear oblateness.
- The desired trajectory geometries and the use wide angle camera causing the other asteroid to appear in the field-of-view (FoV) of the camera.
- Ground operations limit on the turnaround time to a minimum of one day, requiring a higher degree of autonomy for the spacecraft guidance and GNC actions planning.

2.1 IMAGE PROCESSING

In this section, an overall overview of the image processing (IP) software used in Juventas is presented with an emphasis on the IP design and operations for the landing. Two different algorithms are used in Juventas IP, which are both part of the IP baseline of the Hera spacecraft. These algorithms have been proved to work efficiently at the working phase angles (near 90 degrees for the SSTO). These algorithms are:

- Maximum correlation with a Lambertian sphere.
- Centre of Brightness (CoB).

The Lambertian algorithm is the one used for the baseline of the mission, while CoB is only used when pointing at Dimorphos during the landing attempt. For both algorithms, the objective is to autonomously determine the line of sight (LoS) to the center of the asteroid. The use of the Lambertian algorithm was decided as a step up in performance compared to the CoB algorithm without a prohibiting increase in computational load. This choice was made due to the following points:

- (1) CoB introduces sizeable bias with respect to the LoS to the centre of an incompletely imaged disc.
- (2) The shape of Didymos, albeit irregular, it is close to a sphere, thus profiting from the sphere formulation.
- (3) Any illuminated pixels not coming from the asteroid surface (e.g., Dimorphos in FoV, bright stars or planets) will not impact as much the final centroid measurement as in CoB.

In the case of the landing, the design driver was Dimorphos oblateness, which would decrease the performance of lambertian results. It is important to mention however, that an assessment is being performed with the images provided by DART which may conclude that Didymos irregular shape do not sufficiently fit the models used for validating the lambertian algorithm, thus CoB may be used for all mission phases.
To minimize performance degradation during landing due to point (3), the CoB is able to mask the primary body in case it is in the camera FoV and it has a minimum angular separation accounting for spacecraft position uncertainty. To perform the masking and the additional sanity checks performed during the pre-process of the CoB, IP uses the following inputs from the GNC:

- Sun direction in inertial frame.
- SC estimated state in inertial frame relative to Didymos.
- SC estimated covariance in inertial frame.
- Dimorphos state in inertial frame relative to Didymos.
- Quaternion expressing the rotation from camera frame to inertial frame.

The IP algorithm during the landing performs the following sequence:

- Assure Dimorphos is in the FoV.
- Assure Dimorphos is not eclipsed by the main body.
- Compute the worst case of the minimum angular margin between bodies from spacecraft position (using the SC covariance and a tuned uncertainty for Dimorphos position).
- Check that the worst case minimum angular distance is positive.
- Perform image thresholding.
- Perform the masking.
    a. Determine the direction of Dimorphos from Didymos in camera frame (by using SC position and Dimorphos position relative to Didymos).
    b. Compute the furthest illuminated pixel of Dimorphos from Didymos.
    c. Calculate the *base point* (from the furthest point add apparent body size of Dimorphos in pixels plus margin).
    d. Mask the nonvalid pixel zone. This zone is defined from the base point, the image region divided by a perpendicular line to the Didymos-Dimorphos vector in camera frame, where Didymos would lie (Figure 1).
- Perform CoB.
- Correct final measurement for geometric distortion.

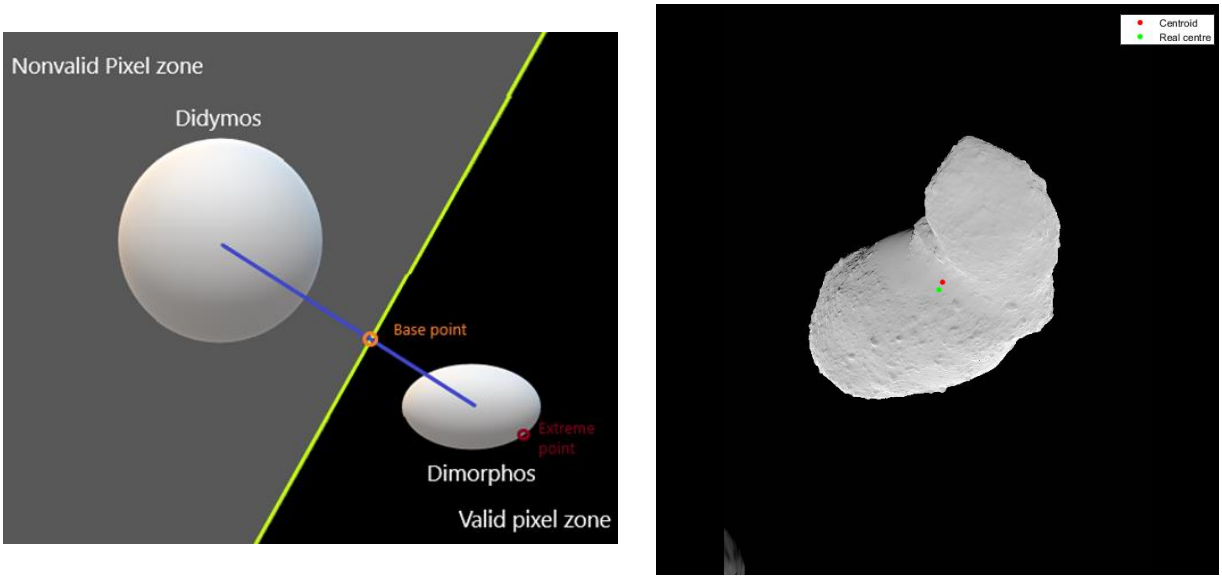

Figure 1. CoB masking. On the left, procedure schematic. On the right, example from landing with Didymos on FoV (bottom-left).

The image processing software receives a greyscale image in a 2048x2048 uint8 format. Then, the respective binning is applied for each algorithm (8:1 binning for lambertian while 4:1 for CoB). A thread in the OBC of Juventas (Linux) is running to check when a new image is posted in memory. The pre-processing of the image is performed before posting it on memory, while the geometric distortion is corrected directly on the output of the image processing.

During the landing, the IP is automatically switched off once the estimated distance to Dimorphos is lower than a threshold (650 m for current reference). This value is tuned and is highly dependent on trajectory geometry. The rationale is to switch off the IP once: performance of IP decreases greatly and/or no sufficient margin is available for masking of Didymos.

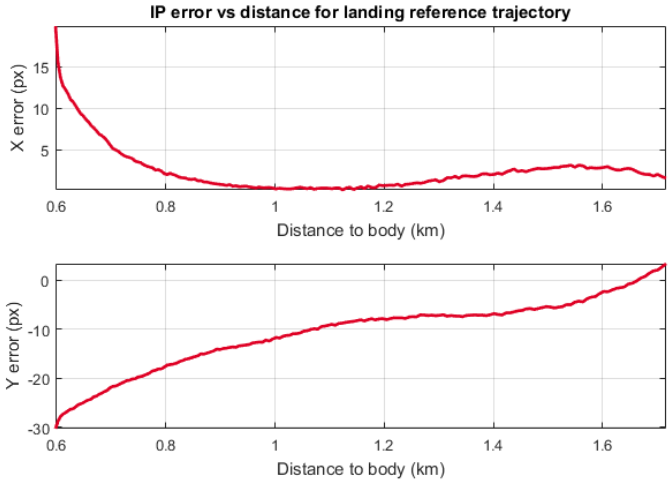

Figure 2. CoB error in pixels as a function of distance to Dimorphos for the landing reference trajectory.

2.2 NAVIGATION FILTER

The purpose of the translational navigation (TNAV) is to perform data fusion with the centroid and range measurements available according to the specific phase and to estimate the relative position and velocity of the spacecraft with respect to the binary asteroid system. The filter is the same for the landing as for the rest of the mission phases, only changing the way the filter pre-processes the measurements. The filter is an EKF that has the following variables and parameters as the augmented state:

- Spacecraft state in Ecliptic J2000 centred in Didymos (6 states).
- Spacecraft non modelled acceleration in Ecliptic J2000 (3 states). This variable absorbs the following uncertainties: gravitational parameters, lower fidelity SRP modelling, SC mass and the effect of non-spherical gravity.
- Bias of lambertian centroid measurement over Didymos expressed in camera frame (2 states). This bias captivates the following effects: shape of Didymos, deviation from centre of mass to geometrical centre and ADCS attitude estimation error.
- Bias of CoB centroid measurement over Dimorphos expressed in camera frame (2 states). This bias captivates the following effects: shape of Dimorphos, deviation from centre of mass to geometrical centre, ADCS attitude estimation error and Dimorphos ephemeris error.
- Bias of range measurement over Didymos (1 state). This bias captivates the following effects: difference between on-board shape model and real shape, altimeter LoS uncertainty (ADCS bias and mounting misalignment) and rotational ephemeris error.
- Bias of range measurement over Dimorphos (1 state). This bias captivates the following effects: difference between on-board shape model and real shape, altimeter LoS uncertainty (ADCS bias and mounting misalignment), rotational ephemeris error and Dimorphos ephemeris error.

These biases may not be constant and can vary in time. To deal with the variation, the augmented states corresponding to the biases are modelled as First Order Gauss Markov (FOGM) processes within the navigation filter. This allows the user to tailor them to the real expected dynamics of the bias. The model for the FOGM in the filter is

$$\dot{b}(t) = -\frac{1}{\tau} b(t) \tag{1}$$

and the covariance evolves in time according to

$$p_b(t) = \exp\left(-\frac{2}{\tau}(t - t_0)\right) p_{b0} + s(t - t_0) \tag{2}$$

where s is the process noise covariance of the FOGM given by

$$s(t - t_0) = \frac{q\tau}{2}\left[1 - \exp\left(-\frac{2}{\tau}(t - t_0)\right)\right]. \tag{3}$$

Since the covariance approaches a finite steady-state value equal to $q\tau/2$ as t becomes infinite, this $q\tau/2$ can be selected as the uncertainty σ^2 of the bias and the initial value p_{b0} can be set as σ^2 as well. This allows for only σ and τ to be tuned. For subsequent steps of the filter, filter covariance can be updated sequentially with (where it has been assumed that $\Delta t \ll \tau$)

$$p_b(t + \Delta t) = -\frac{2\Delta t}{\tau} p_b(t) + \sigma^2\left(1 + \frac{2\Delta t}{\tau}\right). \tag{4}$$

Besides the modelled biases, there are contributors that cannot be estimated and are more similar to white noise. These effects are modelled in the pre-process of the filter and introduced as the covariance of the measurements that are passed in the filter. Noise is driven by the following contributions: attitude determination noise, differences between asteroid real shape and a sphere for centroid and laser noise for range.

For state propagation, Euler method is used, and the following accelerations are considered:

- Central body accelerations from Didymos.
- Third body acceleration from Dimorphos and the Sun.
- SRP as cannonball model.
- Manoeuvre accelerations.

Non-spherical gravity terms were neglected from the filter since their contribution is negligible for the bulk of the mission (SSTOs) and their implementation would quickly escalate the computational cost. This simplification obviously impacts state propagation accuracy during landing.

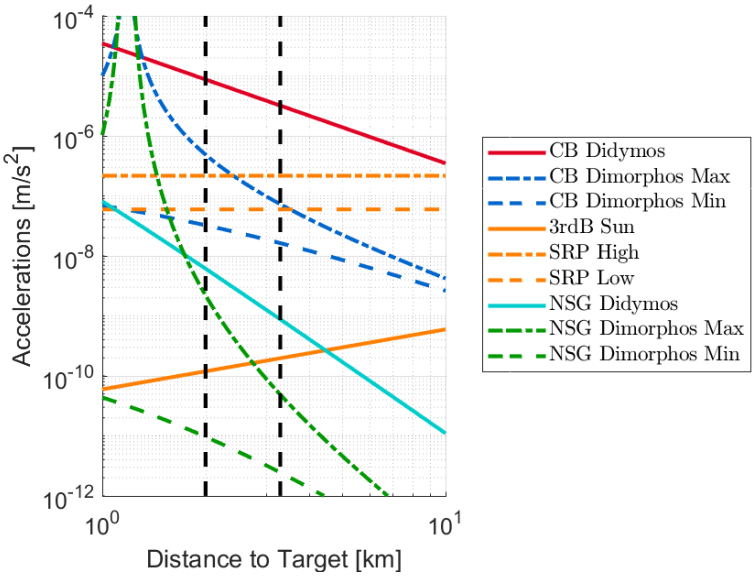

Figure 3. Perturbation magnitude at different distances in the Didymos system.

Regarding measurement prediction models, the filter has two different models implemented for both range estimation and centroid estimation. For range estimation, two different shape models are used:

- Ellipsoid fitting model.
  - Lower fidelity model. (24 coefficients to fit one ellipsoid per asteroid quadrant)
  - Used for computing the observability matrix.
- Triangle mesh model of asteroid surface.
  - Higher fidelity model. (320 triangular faces fitting the surface of each asteroid)
  - Used for computing the expected altimeter measurement to obtain the altimeter residual.

For centroid estimation, the filter models differently Lambertian and CoB centroid measurements:

- Lambertian model: it is computed through the pinhole projection of the estimated geometric centre of Didymos.
- CoB model: it is computed through the pinhole projection plus the addition of the centre of brightness shift along the sun direction d_{shift}. This shift (Eq. 5) assumes a perfect sphere as shape and uses the size of the Dimorphos R_{body} in pixels, the phase angle to the body θ and the sun direction in camera frame u_{sun}.

$$d_{shift} = \frac{4}{3\pi}(1 - \cos\theta)\, R_{body}\, u_{sun} \tag{5}$$

Two different operational modes are implemented for the filter: (1) The filter takes centroid and range measurements whenever these become available. (2) The filter runs in pure propagation ignoring any measurements. Mode (1) is the nominal mode. During this mode the image processing is in synch with the laser rangefinder allowing the GNC to pass simultaneously both a centroid measurement and a mean range measurement (the mean of the last 20 available ranges to decrease noise) to the filter. This timeline is presented in Figure 4.The rationale for linking centroid measurements with range is to ensure that a valid LoS was present when the laser took the measurements. During landing, when no IP is available, range measurements are continuously being processed and sent to the filter. The general logic of range measurement processing is shown in Figure 5. Meanwhile, mode (2) is dedicated to the initial release of Juventas, manoeuvre execution and contingency operations.

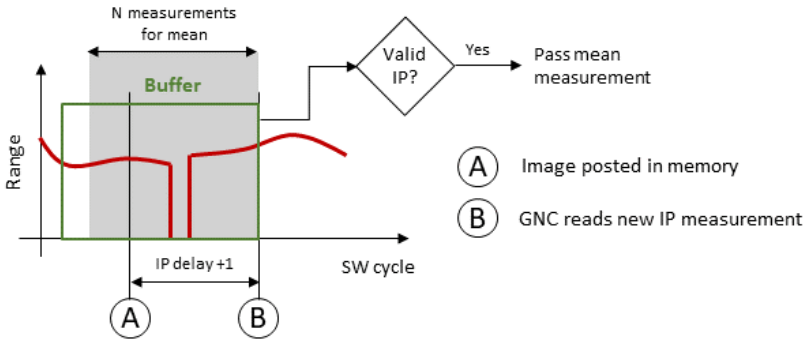

Figure 4. Range measurement timeline during nominal operations.

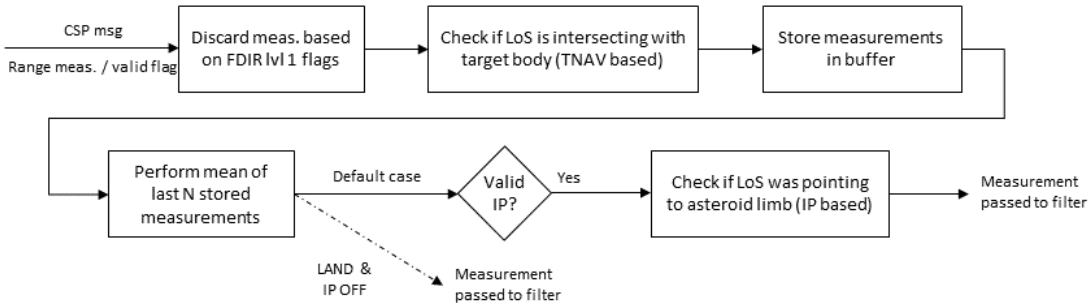

Figure 5. Range measurement pre-process for navigation filter. CSP stands for CubeSat protocol.

2.3 TRANSLATIONAL GUIDANCE

The translational guidance (TGUI) module is in charge of computing the required manoeuvre ΔV in inertial frame. Unless this manoeuvre is a braking manoeuvre for landing, where the trigger is event-based, the output is generated at a predefined on-board time uploaded by ground. The TGUI module allows for some on-board autonomy by updating the value of the required ΔV based on TNAV estimation and a predetermined target position using a fixed time of arrival (FTOA) algorithm.

The FTOA algorithm can be easily found in the literature [8] but as summary, the ΔV correction assumes linearized dynamics by using an STM linking the initial state with the target state and based on initial deviations on position and velocity calculates the new total required ΔV_{CMD}.

$$\Delta V_{CMD} = -\Phi_2^{-1}\Phi_1\,\delta r(t_0) - I\,\delta v^{-}(t_0) + \Delta V_{NOM} \tag{6}$$

where the STM is represented as

$$\Phi(t_f, t_0) = \left[\frac{\partial x(t_f)}{\partial x(t_0)}\right]_{ref} = \begin{bmatrix}\Phi_1 & \Phi_2\\ \Phi_3 & \Phi_4\end{bmatrix} \tag{7}$$

,I represents the identity matrix and ΔV_{NOM} the nominal predefined manoeuvre ΔV.

Additionally, the TGUI implements a function to autonomously compute the required braking manoeuvre ΔV. This module computes the ΔV that achieves the predefined velocity vector relative to Dimorphos. Nominally, this vector has been defined as a norm in the radial direction with respect to Dimorphos, thus removing any lateral velocity and letting the SC free fall downwards.

To tune the TGUI parameters (number of corrective manoeuvres, braking manoeuvre distances to Dimorphos centre and desired velocities after braking) a sensibility analysis was performed to determine the set of parameters with a higher landing probability, resulting in four manoeuvres evenly spaced out and two braking manoeuvres, one at 400 m and 7 cm/s radial velocity and a second one at 150 m with 0 cm/s radial velocity.

3 LANDING SIMULATIONS

3.1 REFERENCE TRAJECTORY

A study from mission analysis was performed to select the most promising landing trajectory to test the GNC on. Two different approaches were studied: a first one consisting of a direct injection from the SSTO and a second one based on the soft-landing techniques which take advantage of the three body dynamics by targeting L2. The direct one was later discarded during the GNC test campaign as it provided lower chances of touchdown. One drawback of this L2 trajectory is that IP is turned off much earlier as Didymos appears in the FoV, slightly increasing the position error from the EKF at the end of the trajectory.

The study consisted of a search on the solution space based on a backwards propagation from L2. The velocity vector at L2 was generated based on the Conley criteria ([9] and [10]). The Conley approach provides, based on the CR3BP theory, directions from L2 to which trajectories have a high probability of landing on the secondary body. Different velocity vectors inside the cone were simulated (Figure 6). Constraints were imposed on landing duration, landing velocity, impact angle and phase angle with respect to both bodies.

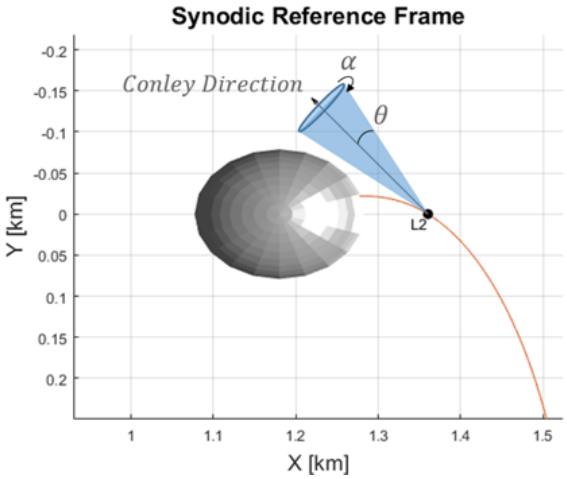

Figure 6. The safety cone from Conley's criteria for propagating the trajectories.

The selected trajectory was the one from all the feasible trajectories that showed one of the lowest insertion ΔV with sufficient margin on landing velocity to the 8 cm/s set as limit (estimated maximum allowable velocity to avoid reaching L1 escape velocity after bounce). The main parameters of the selected trajectory are presented in Table 1 and the trajectory in inertial frame can be seen in Figure 7. This reference trajectory is the one used for the FTOA algorithm.

Table 1: Summary of the selected trajectory parameters.

Landing duration (hours)	5.75
Landing velocity (cm/s)	5.9
Impact angle (deg)	14.2
Insertion ΔV (cm/s)	16.5
Phase Angle Juventas - Didymos (deg)	30.2
Phase Angle Juventas - Dimorphos (deg)	54.9

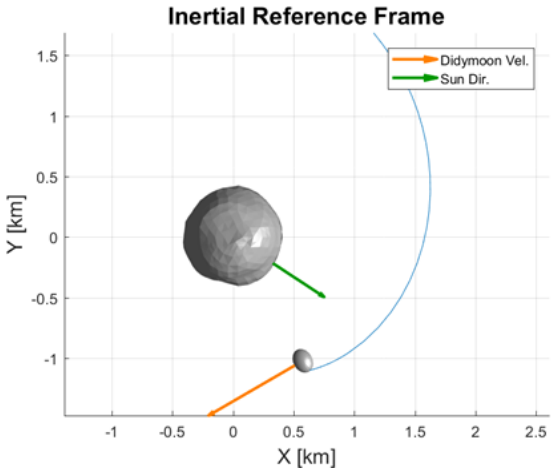

Figure 7. Selected trajectory for the soft-landing approach (using L2).

For the landing scenario, state dispersion is modelled in the following manner:

2. From the pre-manoeuvre state at insertion point, backpropagate the nominal state 2 days (turnaround time) into the SSTO 2 km.
3. Apply the estimated knowledge to cut-off from ground to that final state. No dispersion is applied, only knowledge.
4. Propagate forwards the newly dispersed state up until 2 hours before insertion epoch.

State dispersion at SSTO is modelled with Equinoctial Orbital Elements (EOE) [11] since these set of parameters behave very linearly compared to cartesian state evolution. The knowledge values applied at the SSTO 2 km are presented in Table 2. Since precise shape models do not exist yet of Dimorphos, a scaled version of (25143) Itokawa is used. The baseline for camera acquisition frequency is set to 10 minutes.

Table 2: Knowledge values at cut-off for SSTO 2km in EOE.

Parameter	a (m)	L (rad)	f (-)	g (-)	h (-)	k (-)
3σ	50	0.015	0.02	0.02	0.01	0.01

3.2 MONTE-CARLO RESULTS

A 116 shot Monte-Carlo closed-loop simulation is performed to assess GNC performance during the landing phase. Figure 8 and Figure 9 compare real-world trajectory with the reference trajectory. Figure 8 shows velocity modulus and distance time evolution with respect to Dimorphos while Figure 9 directly reflects the difference between reference and real-world trajectory in cartesian coordinates in the synodic reference frame. It can be observed that for position, the highest dispersion exists in the Z direction at the moment of insertion but it monotonously decreases until the moment of touchdown. This dispersion is due to the true anomaly uncertainty after the two days in SSTO. In Figure 10, TNAV performance can be observed in terms of position error and covariance. Position covariance converges below 20 meters after insertion manoeuvre and slowly increases after IP switch off up to 25 meters. Maximum position error from filter occurs after the first braking manoeuvre reaching 28 m, 40 m and 18 m in the radial, tangential and normal direction respectively. Regarding manoeuvre statistics, Table 3 shows the main manoeuvre parameters. Since an aggressive approach has been selected for the last braking manoeuvre to cancel all velocity, some shots do not manage to achieve the required ΔV. Based on the results, a less aggressive approach could be selected for the final braking, which would reduce reducing free-fall duration as well. With this approach, around 3 cm/s in the radial direction and 1 cm/s is gained in the lateral direction (mean values) resulting in a

mean impact velocity of 51.9 mm/s. Ignoring the shots with uncompleted final braking manoeuvre (would be handled by central software), the landing rate defined as landing impacts below the 8 cm/s limit is 115/116 (99.1%). Figure 11 shows the final landing locations from the simulation (using the scaled version of Itokawa).

Table 3: Monte-Carlo results: manoeuvre statics. (*) 12 out of 116 shots do not finish manoeuvre.

Manoeuvre #	**1 (insertion)**	**2**	**3**	**4**	**Brake 1**	**Brake 2 (*)**
Mean ΔV (mm/s)	165	6.5	3.2	1.1	27.4	60.7
ΔV std. deviation (mm/s)	-	20.5	3.4	4.0	5.5	25.7
Mean duration (s)	1877	206	45	42	390	859
Max. duration (s)	2016	599	122	156	505	1153

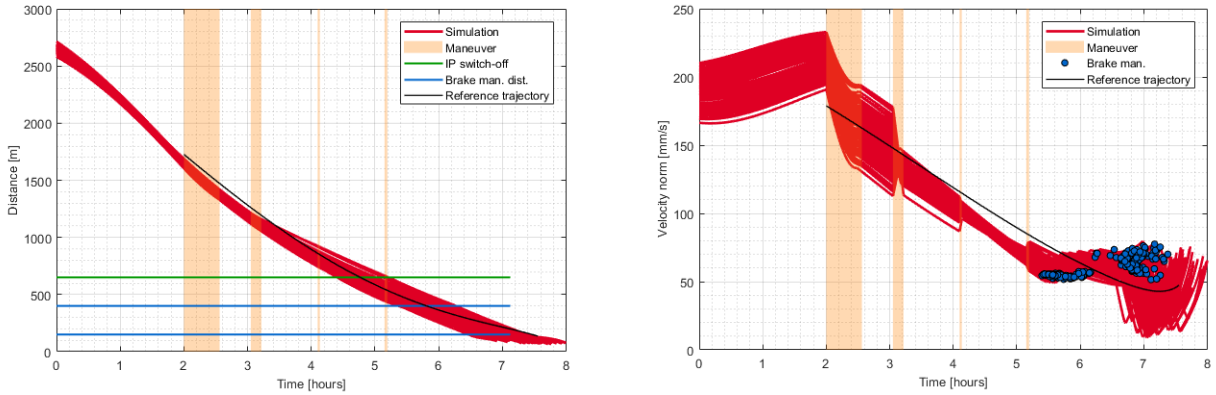

Figure 8. Monte-Carlo simulation results with reference trajectory data and manoeuvre times plotted on top. On the left, SC distance to Dimorphos as a function of time. On the right, velocity modulus with respect to Dimorphos on synodic frame.

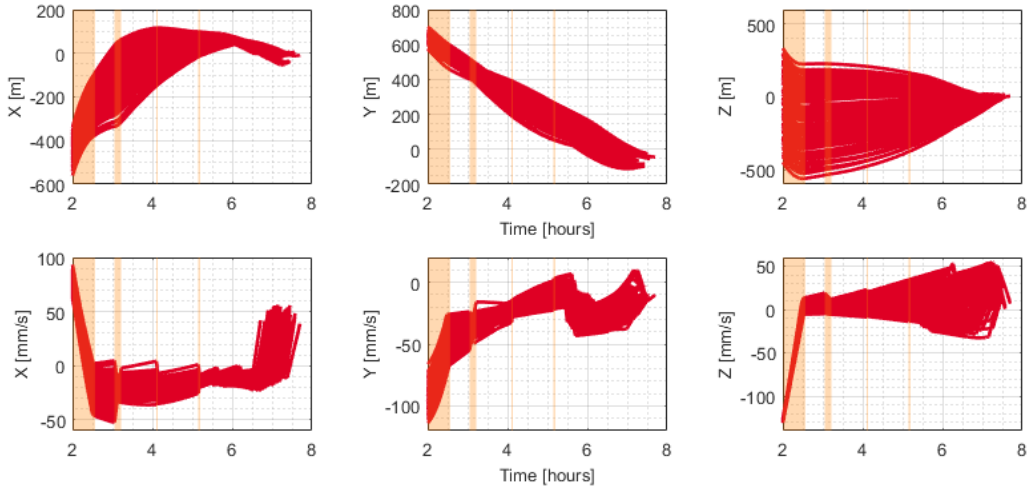

Figure 9. Monte-Carlo simulation results: difference between real-world trajectory and reference trajectory in synodic frame given in cartesian coordinates. Highlighted in orange are manoeuvre times.

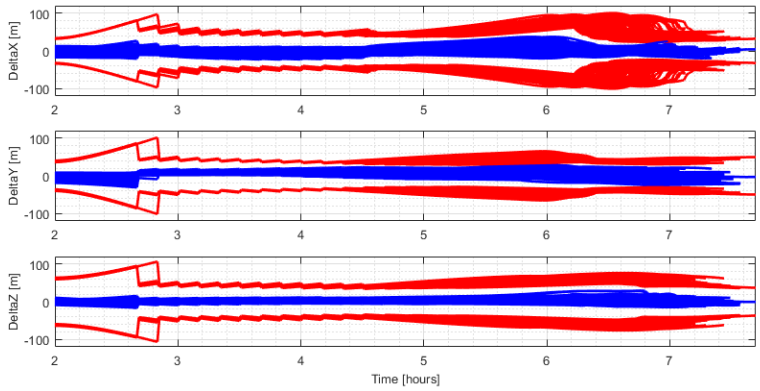

Figure 10. Monte-Carlo simulation results: error in the estimated position (blue) and the estimated 3σ covariance (red) from filter given in inertial frame.

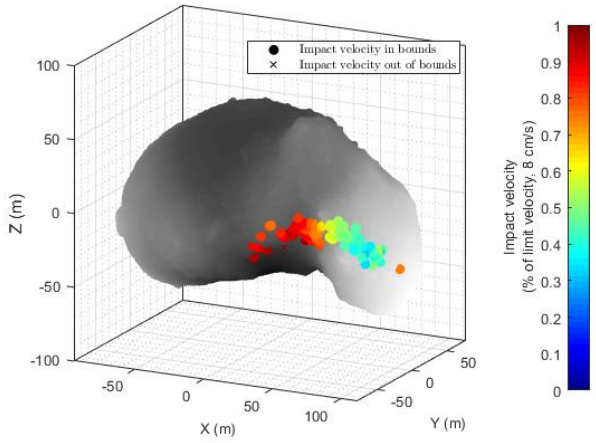

Figure 11. Monte-Carlo simulation results: landing locations in Dimorphos.

4 CONCLUSIONS

This paper provides an overview on the Juventas GNC architecture, developed as part of GMV's role in the Hera mission, focusing on the main adaptations that have been performed for the landing experiment. Highlights on some of the key aspects of the design regarding the navigation filter, image processing and translational guidance are presented. Additionally, the procedure for the soft-landing trajectory generation using the L2 point is summarized. Even with the constraints imposed by the environment: highly perturbed dynamics, oblateness of Dimorphos and prolonged ground turnaround times, the GNC shows some promising results from Monte-Carlo simulations of the landing phase, achieving a near 100% landing rate. Further work can be performed to decrease the dispersion at the insertion from SSTO into the landing trajectory, either on-board or by testing new trajectory approaches, as well as further braking manoeuvre tuning to make the touchdown more efficient in terms of ΔV. Additionally, an updated, more realistic shape model of Dimorphos would be required to properly assess the performance of the GNC during the last part of the descent.

5 DISCLAIMER

The view expressed herein can in no way be taken to reflect the official opinion of the European Space Agency.

6 REFERENCES

[1] Scheeres, D., Sutter, B. and Rosengren, A., *Design, dynamics and stability of the osiris-rex sunterminator orbits*, 2019, Advances in the Astronautical Sciences Vol. 148, pp. 3263–3282.

[2] Hussmann, H. et al., *Stability and evolution of orbits around the binary asteroid 175706 (1996 fg3): Implications for the marcopolor mission*, Planetary and Space Science Vol. 70 nr. 1, pp. 102 – 113, 2012.

[3] Veverka, J., et al. *The landing of the NEAR-Shoemaker spacecraft on asteroid 433 Eros.* Nature 413.6854 (2001): 390-393.

[4] Ritter, Birgit, et al., *Measuring gravity with the GRASS instrument on the Hera mission.* European Planetary Science Congress. 2022.

[5] Kawaguchi, Jun'ichiro, Akira Fujiwara, and Tono Uesugi. *Hayabusa—Its technology and science accomplishment summary and Hayabusa-2.* Acta Astronautica 62.10-11 (2008): 639-647.

[6] Tsuda, Yuichi, et al. *Hayabusa2 mission status: Landing, roving and cratering on asteroid Ryugu.* Acta Astronautica 171 (2020): 42-54.

[7] Lauretta, D. S., et al. *OSIRIS-REx: sample return from asteroid (101955) Bennu.* Space Science Reviews 212 (2017): 925-984.

[8] Battin, Richard H. *An introduction to the mathematics and methods of astrodynamics*. Aiaa, 1999.

[9] Tardivel, Simon, and Daniel J. Scheeres. *Ballistic deployment of science packages on binary asteroids.* Journal of Guidance, Control, and Dynamics 36.3 (2013): 700-709.

[10] Conley, C. C. *Low energy transit orbits in the restricted three-body problems.* SIAM Journal on Applied Mathematics 16.4 (1968): 732-746.

[11] Walker, Michael JH, B. Ireland, and Joyce Owens. *A set modified equinoctial orbit elements.* Celestial mechanics 36.4 (1985): 409-419.